ACS APPLIED MATERIALS & INTERFACES

Research Article

www.acsami.org

Light-Concentrating Plasmonic Au Superstructures with Significantly Visible-Light-Enhanced Catalytic Performance

Jinhu Yang,*[,†,‡] Ying Li,[†] Lianhai Zu,[†] Lianming Tong,[§] Guanglei Liu,[†] Yao Qin,*[,‡] and Donglu Shi*[,‡,∥]

[†]Department of Chemistry, Tongji University, Siping Road 1239, Shanghai 200092, People's Republic of China

[‡]Research Center for Translational Medicine & Key Laboratory of Arrhythmias of the Ministry of Education of China, East Hospital, Tongji University School of Medicine, No. 150 Jimo Road, Shanghai 200120, People's Republic of China

[§]Institute of Physics Chinese Academy of Sciences, Beijing 100190, People's Republic of China

[∥]Materials Science and Engineering Program, Department of Mechanical and Materials Engineering, College of Engineering and Applied Science, University of Cincinnati, Cincinnati, Ohio 45221, United States

Supporting Information

ABSTRACT: Noble metals are well-known for their surface plasmon resonance effect that enables strong light absorption typically in the visible regions for gold and silver. However, unlike semiconductors, noble metals are commonly considered incapable of catalyzing reactions via photogenerated electron–hole pairs due to their continuous energy band structures. So far, photonically activated catalytic system based on pure noble metal nanostructures has seldom been reported. Here, we report the development of three different novel plasmonic Au superstructures comprised of Au nanoparticles, multiple-twinned nanoparticles and nanoworms assembling on the surfaces of SiO_2 nanospheres respectively via a well-designed synthetic strategy. It is found that these novel Au superstructures show enhanced broadband visible-light absorption due to the plasmon resonance coupling within the superstructures, and thus can effectively focus the energy of photon fluxes to generate much more excited hot electrons and holes for promoting catalytic reactions. Accordingly, these Au superstructures exhibit significantly visible-light-enhanced catalytic efficiency (up to ~264% enhancement) for the commercial reaction of p-nitrophenol reduction.

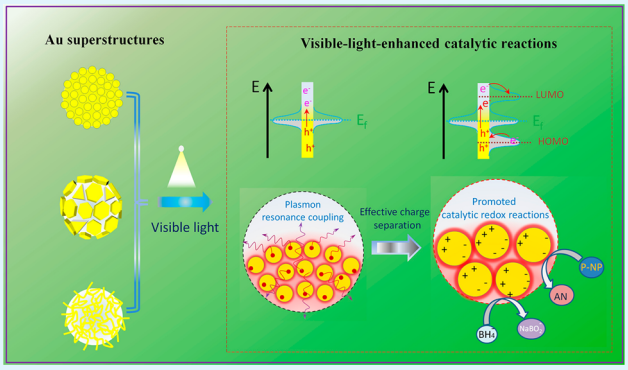

KEYWORDS: *noble metal, Au plasmonic superstructures, light concentration, visible-light-enhanced catalytic reactions*

INTRODUCTION

Noble metals are important catalysts playing a critical role in industrial catalysis, environmental purification, and new energy development.[1−7] As is well-known, noble metals are rare and cost-ineffective, which has limited their industrial applications in the past century. Extensive research has been carried out to improve their catalytic efficiency and develop alternative materials.[8−11] In metal-catalyzed redox reactions, metals serve as catalytic centers that transfer electrons between two targeting molecules by dynamically forming/decomposing metal-based intermediates.[12−20] In contrast, photocatalysis over semiconductors driven by sun light is a green, low-cost, and efficient method for solar energy as it is clean and abundant in nature.[21,22] In a typical photocatalysis process, photoinduced electron–hole pairs can be effectively separated in the conduction and valence bands of semiconductors to catalyze the redox reactions, respectively. For noble metals, it is well-known that the "hot electrons" of conduction band can be excited by surface plasmon excitation.[23−28] The electron–hole pairs through interband transitions can also be generated by absorbing photons of appropriate energies[29,30] However, these electrons and holes incur a much higher recombination rate than that in semiconductors because of the continuous energy band structure of noble metals. Therefore, noble metals are considered inert for efficiently utilizing light energy to catalyze reactions. By far, noble metals have been involved mainly in either the light-absent catalytic system as pure metal catalysts[31−34] or the photocatalytic system as composite catalysts to enhance the charge separation of semiconductors.[35−39] However, it has been a great challenge to utilize light energy directly to initiate or promote catalytic reactions using nanostructured pure noble metals, similar to the role of semiconductors in conventional photocatalysis.

Nanostructured noble metals with specific size, shape, and assembly have attracted high attention for their structure-modulated surface plasmon resonance (SPR) properties and important applications.[31−51] For example, Au-based nanocages exhibit higher catalytic activity than their nanobox and

Received: February 4, 2015
Accepted: April 3, 2015
Published: April 3, 2015

DOI: 10.1021/acsami.5b01078
ACS Appl. Mater. Interfaces 2015, 7, 8200−8208

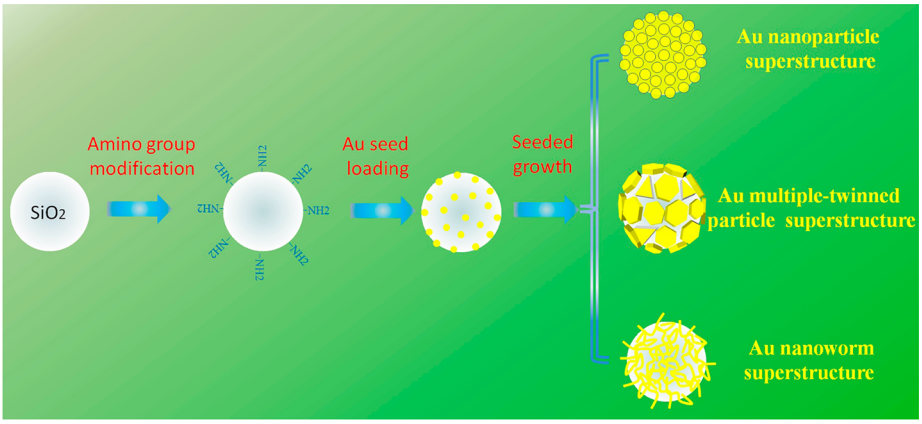

Figure 1. Schematic illustration of the synthetic route for Au superstructures.

nanoparticle counterparts in the catalytic reduction of p-NP.[34] Furthermore, the combination of atomic-scale Au clusters and nanoscale Au particles can integrate the catalytic and plasmonic property for in situ surface-enhanced resonance scattering (SERS) monitoring of chemical reaction.[46] Particularly, plasmonic Ag nanostructures with visible light excitation and thermal energy stimulus are capable of reducing O_2 to O_2^-, facilitating the catalytic oxidation reactions.[40] This indicates a high possibility of visible-light triggered catalytic reactions over pure noble metals, for example, by means of nanostructural design.

In this work, three different novel Au superstructures including Au nanoparticles (NPs), Au multiple-twinned particles (MTPs) and Au nanoworms (NWs) arrayed on the surfaces of SiO_2 nanospheres have been developed via a well-designed synthetic strategy. Briefly, the synthetic process involves three steps: surface modification of SiO_2 nanospheres with amino groups, Au nanoseed loading on amino group-modified SiO_2 nanospheres, and subsequently seeded epitaxial growth of various Au nanostructures on SiO_2 nanospheres directed by additives of poly(vinylpyrrolidone) (PVP) and different reductants (Figure 1). The ordered dense assembly of Au nanostructures can effectively facilitate strong broadband light absorption and improve light energy harvesting of Au catalysts because of plasmon resonance coupling. The energy of photon fluxes can be well-concentrated in the plasmonic Au superstructures for generating much more excited hot electrons and oppositely charged counterparts that promote catalytic reactions. Because of the unique structures and photoelectric properties, these Au superstructures display highly visible-light-enhanced catalytic performance in the reduction of p-NP. The significance of this work includes: (i) the plasmonic metal superstructures harnessing only sunlight can significantly enhance the catalytic efficiency of important commercial reactions at room temperatures. These superstructures pave a new way to the catalytic technology of metal catalyst-involved reactions and the development of relevant catalytic industry; (ii) noble metals, which are traditionally considered to be inert for light-driven photocatalytic reactions, are able to trigger catalytic reactions like semiconductors. This will help to deeply understand the different photocatalytic reaction mechanism over pure noble metals relative to conventional semiconductors; and, (iii) the investigation on novel Au superstructures establishes the correlation between the advanced assembly forms of metal nanostructure and their SPR-related photoelectric property. This will benefit the rational design of novel metal nanostructures in achieving desirable properties for specific applications.

EXPERIMENTAL SECTION

Synthesis of Amino Group-Modified SiO_2 Nanospheres. SiO_2 nanospheres (diameter = 220 nm) were synthesized in an ethanol–water system according to our previously reported method.[45] This synthetic method was derived from the classic Stöber method that employed an ethanol-ethyl ester system.[41] Briefly, 3.263 g of 28% (w/w) ammonia and 9.8 mL of H_2O were added into 126.8 mL of ethanol with stirring for 30 min. Then, 6.25 g of tetraethyl orthosilicate was injected, forming an opalescent reacting solution. After reaction for 22 h under stirring, the produced SiO_2 nanospheres were collected by centrifugation and washed with ethanol 3 times. Subsequently, 0.15 g of the as-prepared SiO_2 spheres was redispersed in 90 mL of ethanol, followed by injection of 40 μL of 3-aminopropyltriethoxysilane (APTES). The mixture was kept in an oil bath at 80 °C for 3 h, and then washed with water 3 times through centrifugation. Finally, the aminated SiO_2 spheres were prepared and dispersed in ethanol (7.8 mg/mL) as a stock solution.

Preparation of SiO_2@Au Seed Nanoparticles. The synthesis was conducted according to the methods[45] reported previously with modifications. Au seeds ($d \approx 5$ nm) were prepared beforehand by mixing 550 μL of $HAuCl_4$ (50 mM) and 2 mL of sodium citrate (1% w/w) in water (90 mL), and subsequently adding of 1 mL of sodium citrate (1% w/w) containing fresh $NaBH_4$ (0.075% w/w) with stirring for 5 min. To begin the experiment, we added 800 μL of the aminated SiO_2 nanosphere stock solution into 25 mL of ethanol, followed by the dropwise injection of 30 mL of as-prepared Au seed solution. Upon continuously stirring for 20 h, the product of Au seed-loaded SiO_2 nanospheres was collected, washed, and redispersed in water (20 mL) for use.

Preparation of Au NP Superstructures. Five milliliters of the SiO_2@Au seed solution was added to 15 mL of water, followed with the addition of 0.25 g of PVP (M_w = 40 000) and 0.05 g of hydroxylamine hydrochloride. Subsequently, 10 mL of $HAuCl_4$ (3 mM) was added in drops, resulting in a gradual color shift from white yellow to black. The reactant solution was stirred at room temperature for 15 h. Finally, the product was washed with water 3 times after centrifugation.

Preparation of Au MTP superstructures. Five milliliters of the SiO_2@Au seed solution was added to 15 mL of water, followed with the addition of 0.25 g of PVP and 0.0126 g of sodium citrate. Subsequently, 10 mL of $HAuCl_4$ (3 mM) was added in drops, accompanied by a gradual color shift from white yellow to black green. The reactant solution was stirred at room temperature for 3 h.

Preparation of Au Worm Superstructures. Five milliliters of the SiO_2@Au seed solution was added to 15 mL of water, followed with the addition of 0.1 g of PVP and 0.15 g of sodium citrate.

DOI: 10.1021/acsami.5b01078
ACS Appl. Mater. Interfaces 2015, 7, 8200–8208

Subsequently, 3 mL of $HAuCl_4$ (3 mM) was added in drops. The reactant solution was stirred at room temperature for 14 h.

Characterization. The morphology was characterized using a scanning electron microscope (SEM, Hitachi S4800, 3 kV) and high-resolution transmission electron microscopy (HR-TEM, JEM 2011, 200 kV). The crystal structure was determined by X-ray diffraction (XRD) using a D/max2550VB3+/PC X-ray diffractometer with Cu Ka radiation with a 1.5418 Å wavelength. A beam voltage of 40 kV and a 100 mA current beam were used. The UV−vis spectra of the samples were recorded on a Cary-50 UV−vis spectrophotometer. The visible light source is a 150 W Xe lamp equipped with an AM 1.5G filter, calibrated with a standard Si solar cell to simulate AM 1.5 illumination (100 mW/cm^2) (model 91160, 300 W, Newport, USA, Full Spectrum Solar Simulator). X-ray photoelectron spectroscopy (XPS) investigation was conducted in PHI-5000C ESCA system (Perkin−Elmer) with Mg Kα radiation ($h\nu$ = 1253.6 eV). The XPS spectra of the studied elements were measured with a constant analyzer pass energy of 46.95 eV. All binding energies (BEs) were referred to the C 1s peak (284.6 eV) arising from surface hydrocarbons (or adventitious hydrocarbon). The content of Au element in Au superstructures was measured by an inductive coupled plasma emission spectrometer (ICP-MS) (PerkinElmer Optima 8000).

Catalytic Property Evaluation of the Au Superstructures under Dark and with Visible-Light Irradiation. One hundred microliters of *p*-nitrophenol (5 mM) and 1 mL of fresh $NaBH_4$ (200 mM) solution were mixed and diluted with water to 3.7 mL, giving a transparent light yellow solution. Then, 3.0 mL of the solution was transferred to a quartz cuvette and measured by a UV−vis spectrometer (Varian Cary 500) to record the initial absorbance. Subsequently, 30 μL of Au superstructure stock solution was injected to catalyze the reducing of p-nitrophenol. For comparison, the catalytic reactions were conducted in dark or under visible light irradiation (wavelength <420 nm was filtered out) with a total maximum intensity of 100 mW/cm^2 (1 solar intensity). The absorbance of reaction solution was recorded in situ at every 2 min until the catalytic reaction is completed.

RESULTS AND DISCUSSION

Figure 2 gives the structure and morphology characterizations of Au NP superstructures evolved from the amino-modified SiO_2 nanosphere templates. SiO_2 nanospheres in Figure 2a show clean smooth surfaces with an average size of ~220 nm. Upon loading of the Au seeds, a layer of uniform yet sparse coverage of 5 nm Au NPs is obtained (Figure 2b), indicating successful Au seed deposition on SiO_2 nanospheres. The SiO_2 nanosphere-supported Au seeds served as the stable nucleation sites for the subsequent controlled growth of various Au shells consisting of NPs, MTPs and NWs, as $HAuCl_4$ was fed in the presence of PVP and different reductants. SEM image in Figure 2c shows core−shell SiO_2@Au NP composites formed at high hydroxylamine hydrochloride concentration after 14 h growth. The SiO_2@Au composites exhibit uniform size and dispersion with a densely coverage of the Au NPs. The magnified SEM image gives closer observation, as shown in Figure 2d. It can be seen that the Au NPs experience considerable growth to a size estimated to be about 20 nm and assemble into single layers, leading to formation of dense Au shells on the SiO_2 sphere cores. The XRD pattern of the SiO_2@Au composites in Figure S1 in the Supporting Information shows a set of broad peaks corresponding to (111), (200), and (220) reflections of the face-centered cubic (fcc) structure of metallic gold (JCPDS Card No. 04−0784). This is mirrored by the corresponding energy-dispersive X-ray spectroscopy (EDS) spectrum, where the Au element is detected, in addition to the elements of Si, O, and C, which come from SiO_2 nanospheres (Figure S2a, b in the Supporting Information). Furthermore, X-ray photoelectron spectroscopy (XPS), which is very sensitive to the oxidation state of gold (e.g., Au^{3+}, Au^+, and Au^0), has been used to characterize the product. As shown in Figure S2c in the Supporting Information, the binding energies of the photoelectron peaks at 333.8 (Au 4d5/2), 352.1 (Au 4d3/2), 546.3 (Au 4p3/2), 642.2 (Au 4p1/2), and 761.0 eV (Au 4s) are characteristic of the Au^0 phase, according to the XPS handbook, confirming the formation of zero-valence gold. Moreover, TEM images also reveal the single-layer Au shells ($d \approx 20$ nm) on the SiO_2 nanospheres in a densely fashion (Figure 2e, f), which is consistent with the SEM observation. At a high resolution, a single Au NP from shell shows continuous lattice fringes with a *d*-spacing of 0.202 nm, corresponding to (200) plane of fcc gold (Figure 2g). The above results suggest the successful formation of SiO_2@Au NP composites with a uniform surface distribution of the Au nanoparticles.

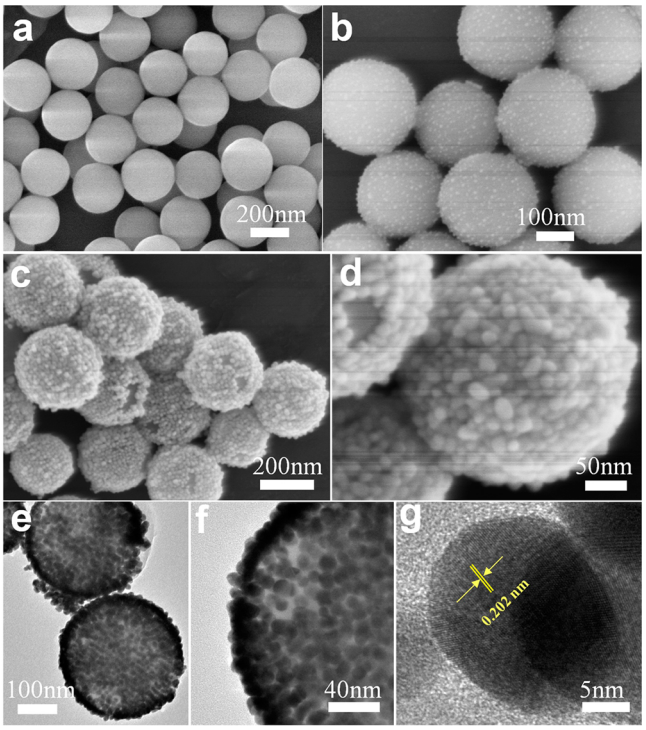

Figure 2. (a, b) SEM images of (a) amino-modified SiO_2 and (b) Au seed-loaded SiO_2 spheres. (c, d) SEM and (e−g) TEM images of SiO_2@Au NPs.

Sodium citrate, a commonly used reductant for shape-controlled synthesis of Au nanocrystals, was chosen instead of hydroxylamine hydrochloride for the synthesis and assembly of Au MTPs and NWs on SiO_2 nanospheres. Figure 3 presents the core−shell SiO_2@Au MTP composites formed in the presence of sodium citrate and PVP. In contrast, the composites of SiO_2@Au MTPs show a larger average diameter of ~300 nm and relatively rough surface (Figure 3a). The MTPs mainly take hexagonal or trigonal symmetries with sizes ranging from 50 to 80 nm (Figure 3a, inset). Unlike Au nanoparticles, the Au MTPs are epitaxially grown and disorderly assembled on the curved surfaces of SiO_2 spheres. Moreover, some quasi-platelike or irregular Au nanoparticles are formed from incomplete growth of Au MTPs, confirmed by the high-magnification SEM image in the inset of Figure 3a. This is likely associated with the disordered assembly of Au MTPs. The corresponding TEM image in Figure 3b confirms that the shells of the composites comprise platelike Au nanocyrstals. A gold MTP on SiO_2

DOI: 10.1021/acsami.5b01078
ACS Appl. Mater. Interfaces 2015, 7, 8200−8208

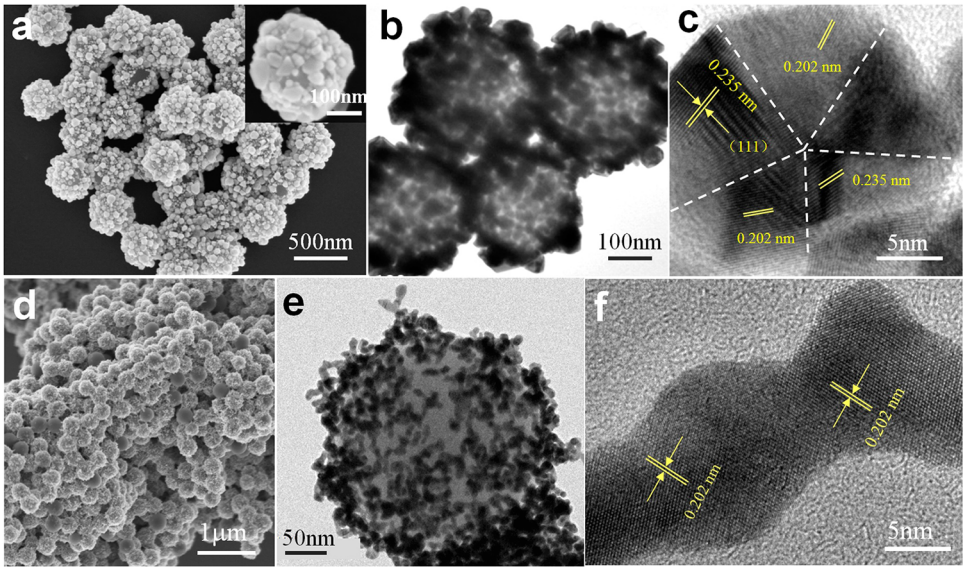

Figure 3. (a) SEM and (b) TEM images of SiO_2@Au MTP composites. (c) HRTEM image of a single Au MTP. (d) SEM and (e) TEM images of SiO_2@Au NW composites. (f) HRTEM image of a single Au NW. Inset of a is the enlarged SEM image of a SiO_2@Au MTP composite.

nanospheres was randomly selected for high-resolution TEM observation and displayed a 5-fold twined crystal structure. As shown in Figure 3c, the MTP is divided into five regions with distinct crystal lattice orientations and different *d*-spacing distances, for example, 0.235 and 0.202 nm as labled corresponding to Au {111} and {200} planes, respectively. The multiple twinned crystal structure makes it impossible to indentify an exact crystal plane of the surface plate. The mechanism responsible for the MTP grown from the primary NPs is still unclear in this work, which is considered to be synergistically controlled by PVP and citrate molecules. The Au MTPs with energy-unstable surfaces can be endowed with high activity in catalytic reactions.[33]

As shown in Figure 3d–f, novel SiO_2@Au NW composites were prepared at a lower PVP concentration (0.1 g/L) and a higher sodium citrate concentration (0.15g/L), relative to the condition for preparation of the SiO_2@Au MTPs. Figure 3d shows that the SiO_2@Au NW composites are prepared on a large scale with uniformly surface distributed Au NWs (Figure 3d and Figure S3 in the Supporting Information). The electronic differection (ED) pattern obtained in an observable area (in set of Figure S3a in the Supporting Information) gives a set of reflection rings corresponding to cubic structured gold (JCPDS Card No. 04–0784), indicating well-crystallized Au NWs. Further, it can be seen that these Au NWs consist of interconnected nanoparticles with sizes of ~20 nm (Figure 3e, f). The integration of Au nanoseeds, mediated by PVP and sodium citrate, leads to the formation of wormlike Au nanostructures, as they are originated from the growth of the initial Au nanoseeds. Meanwhile, the assembly of the Au NWs on SiO_2 sphere surfaces is responsible for the formation of the core–shell SiO_2@Au NWs. To the best of our knowledge, this is the first report of the successful assembly of nonspherical metal nanocrystals on highly curved surfaces of SiO_2 nanospheres, which is the key to the development of Au MTP and Au NW superstructures.

The optical properties were investigated on the Au superstructures, the Au seed colloids, and Au seed-loaded SiO_2 spheres (SiO_2@Au seeds). The corresponding UV–vis spectra of the samples are shown in Figure 4a. It is found that there are obvious red shifts of SPR peaks from ~520 to ~780 nm for different samples, that is, ~520 nm for Au seed colloids, ~530 nm for SiO_2@Au seeds, ~570 nm for Au NW superstructures, ~610 nm for Au MTP superstructures, and ~780 nm for Au NP superstructures, respectively. Meanwhile, there are gradual SPR band broadennings with the same tendency for these Au-based samples: ~30 nm of peak width of Au seed colloids, ~50 nm of SiO_2@Au seeds, ~300 nm of Au NW and Au MTP superstructures, and the entire visible band of Au NP superstructures, respectively. The red shift and broadennings of SPR peaks of the Au superstructures are also well-mirrored by the gradual color change of their aqueous samples. As shown in Figure 4b, optical pictures of the samples show a gradual color change from red to pink, green, and black, which is in good agreement with the UV–vis extinction spectra. The SPR redshifts and peak broadenings are direct evidence of the plasmonic coupling between the primary gold nanostructures in the dense assembly on the surface of SiO_2,[25,27] indicating strongly intensified absorption and high light energy utilization of the Au superstructures.

The catalytic reduction reactions of *p*-nitrophenol (p-NP) based on three Au superstructures under dark and visible-light irrediation were investigated at 25 °C, as shown in Figure 4c–f. Figure 4cm d presents the extinction spectra of p-NP at different times during the reduction process catalyzed by Au NP superstructures. The disappearance of the peak (400 nm) for p-NP indicates the reduction of $-NO_2$ into the $-NH_2$ groups.[34] The significantly improved catalytic rate over Au NP superstructures under visible-light irradiation (Figure 4d) is observed in comparison with that conducted under dark (Figure 4c). The quantative comparisons of the catalytic performance for the three superstructures under dark and visible light are illustrated in Figure 4e, f, respectively. The catalytic reaction rates under dark for the Au NP, Au NW, and Au MTP superstructures are 0.05023, 0.08242, and 0.27223 min^{-1}, respectively (Figure 4e). Their catalytic performaces follow the order: Au NP superstructures < Au NW superstructures < Au MTP superstructures. The catalytic performance differences are found to be associated with the specific structures of different Au primary nanostructures.[34] The

DOI: 10.1021/acsami.5b01078
ACS Appl. Mater. Interfaces 2015, 7, 8200–8208

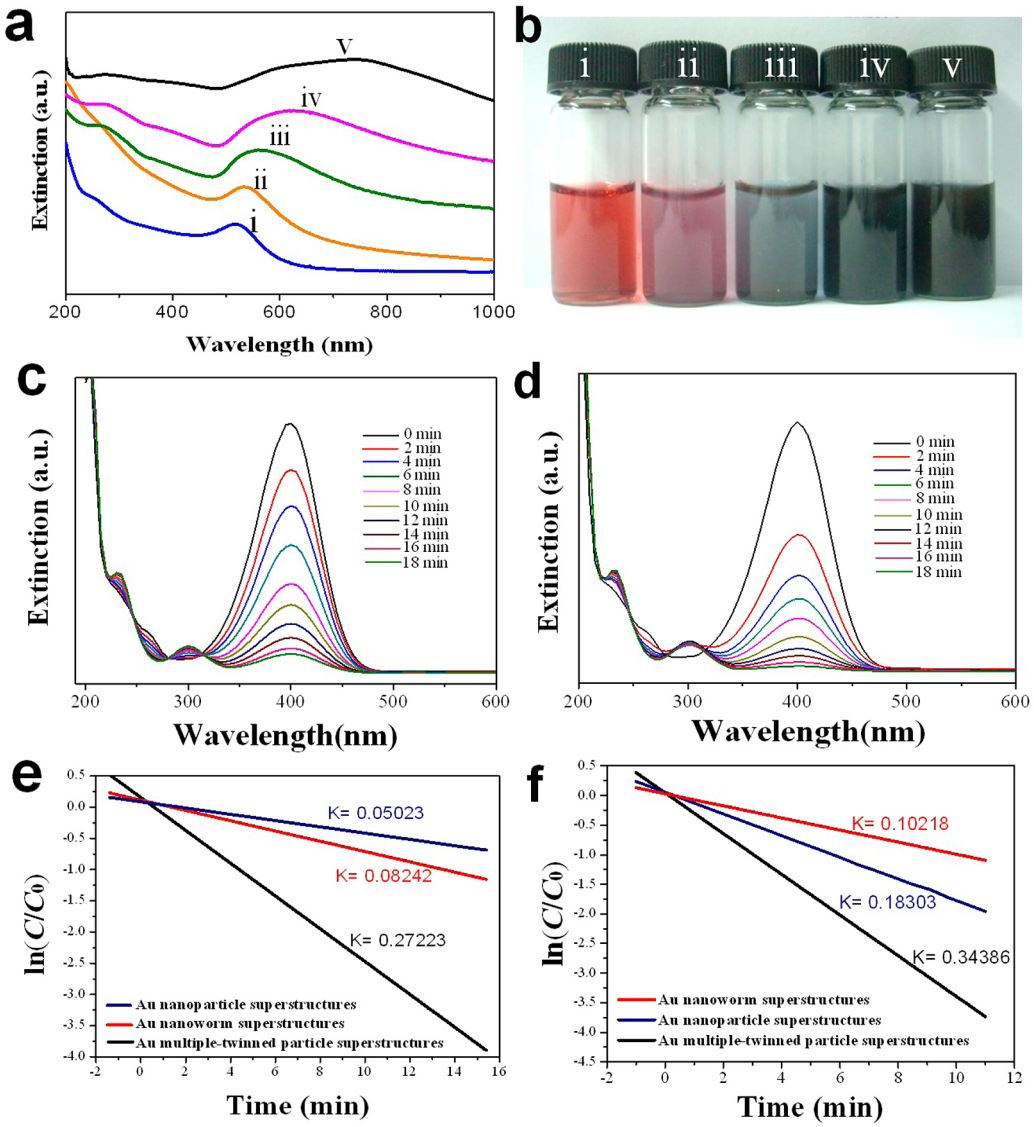

Figure 4. (a) UV−visible extinction spectra and (b) optical color evolution of Au seed colloids, Au-seed-loaded SiO_2 nanospheres, and Au superstructures. (i) Au seed colloids, (ii) SiO_2@Au seeds, (iii) Au NW superstructures, (iv) Au MTP superstructures, and (v) Au NP superstructures. (c, d) Extinction spectra of *p*-nitrophenol as a function of the degradation time recoreded under (c) dark and (d) visible light using Au NP superstructures as the catalyst. (e, f) Catalytic properties of three catalysts of the Au superstructures under (e) dark and (f) visible light. The absorbance of reaction solution was measured every 2 min.

anisotropically structured Au MTPs with exposed active crystal planes display higher catalytic activity than the isotropically structured Au NPs and NWs which were formed from Au nanoparticle intergration. Interesingly, when visible light irradiation is on, the reaction rates of p-NP reduction over the three catalysts are all enhanced, for instance, reaching 0.18303 min^{-1} for the Au NP superstructures, 0.10218 min^{-1} for the Au NW superstructures and 0.34386 min^{-1} for the Au MTP superstructures (Figure 4f). The corresponding catalytic reaction rates are increased by 264.4%, 24.0% and 26.3%, respectively, basically following the order of the light absorption capacities of the three catalysts. For comparison, the p-NP reduction reaction was also conducted in the absence of the Au superstructure catalysts under dark and visible light irradiation (Figure S3 in the Supporting Information). It is found that the reduction of p-NP is still not completed even after 100 min reaction (Figure S4a, b in the Supporting Information) and there is only negligible influence of visible light on the reaction (Figure S4c in the Supporting Information).

The Au amount of the three superstructures used in the catalytic reduction of p-NP was measured by ICP-MS and the results are shown in Table S1 in the Supporting Information. The concentrations for the three superstructured catalysts are 99.95 mg L^{-1} (Au NP superstructures), 86.83 mg L^{-1} (Au MTP superstructures), and 139.07 mg L^{-1} (Au NW superstructures), respectively. It can be found that the Au MTP superstructures with the lowest concentration showed the highest catalytic performance under both conditions of dark and visible light, which should be acribed to their exposed active crystal planes with high reactivity. On the contrary, the Au NW superstructures with the highest concentration yet delivered the worst performance under visible light, probably due to their relatively inert crystal planes and especially poor coverage of Au nanaoparticles on the SiO_2 nanosphere, which limits their efffective utilization of light energy (Figure 4a, cuver

DOI: 10.1021/acsami.5b01078
ACS Appl. Mater. Interfaces 2015, 7, 8200−8208

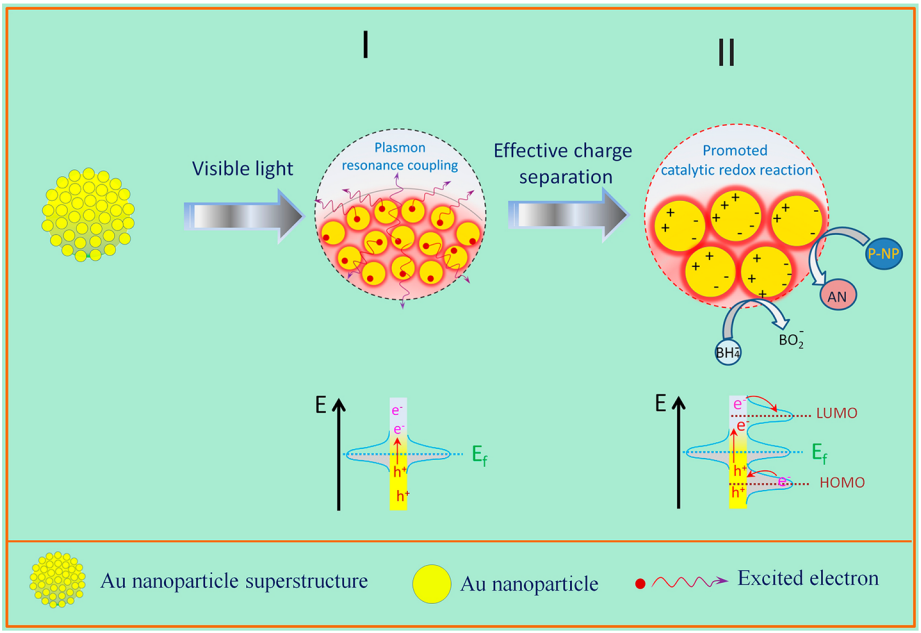

Figure 5. Mechanism responsible for visible-light-enhanced catalytic performance based on Au superstructure catalysts. Step I: Surface plasmon resonance coupling (top) with electron excitation (bottom) on Au superstructure surface under visible light irrediation. Step II: Electron/hole separation (top) on Au superstructure surface and their interband transferring (bottom) between Au catalysts and reactant molecules for promoted catalytic reduction reaction of p-NP.

(iii). In a word, the overall catalytic efficiency of these light-concentrating Au superstructured catalysts depends on both the exposed crystal plane activity of Au primary crystals and the light absorptivity of their advanced architectures.

The recycling catalytic performance for p-NP reduction over Au superstructured catalysts under visible light has been conducted, taking Au NP superstructures as an example. As shown in Figure S5 in the Supporting Information, The reaction rate of p-NP reduction at the first cycle is 0.16816 min^{-1}, whereas it drastically decreases to 0.05514 and 0.03392 min^{-1} at the second and third cycle, respectively. It is found that some Au nanoparticles fell off SiO_2 nanospheres with cycling after repeated centrifuge−dispersion processes (see SEM image of Figure S6 in the Supporting Information). This will result in the damage of the Au superstructures and the aggregation of Au nanoparticles in solution. Both of these are disadvantageous for catalytic reaction, thus leading to the poor recycling performance. To get more stable Au superstructured catalysts with better recycling performance, mercapto-modified SiO_2 can be selected in the future synthesis instead of aminated SiO_2, because of stronger interactions between Au nanoparticles and mercapto groups.

It is noted that a series of commercial metal nanoparticles (Cu, Co, Ni, and Fe) that were embedded in smart hydrogels or cryogels through novel in situ preparation routes have been reported by Sahiner N. et al. and investigated with the catalytic performance for p-NP reduction.[52−54] The novel metals/gels composite catalysts showed great potential in commercial reaction catalysis, dye degradation, and hydrogen generation, with advantages of low cost, cataytic stability, and recyclability. In contrast, the Au superstructures in this work not only serve as efficicent catalysts for normal catalytic reactions under dark conditions, but also represent a class of novel light-sensitive catalysts with remarkable visible-light-enhanced catalytic performance. Moreover, the materials of this light-concentrating superstructure are not limited to the Au element; it is possible to extend to other metals with SPR effect, for example, noble metals of Ag, Pt, and commmerical metals of Cu, etc.

In Au-catalyzed p-NP reduction, Au catalyst served as electron transfer media from reductant molecules such as $NaBH_4$ to p-NP molecules. It was found in our experiment that introducing visible light to the catalytic system could accelerate catalytic reaction. Evidently, the prepared Au superstructures are responsible for the visible-light-enhanced catalytic performance because of their strong plasmon resonance coupling with increased light energy utilization. To further probe the driving force in reaction energy, we calculated the activation energies (E_a) for the catalytic reactions under dark and visible light. The designed catalytic reactions at three different temperatures were conducted for E_a calculations, taking SiO_2@Au NPs catalyzed p-NP reduction reaction as an example. Figures S7 and S8 in the Supporting Information show extinction spectra of *p*-nitrophenol as a function of the degradation time at three different temperatures under dark and visible light, respectively. The results are plotted in Figure S9 in the Supporting Information and the data are also shown in Table S2 in the Supporting Information. E_a under dark and visible light for the catalytic reaction was calculated to be 50.61 and 42.31 kJ mol^{-1}, respectively. This manifests a lower E_a in a visible-light-involved system, giving rise to a higher reaction rate.[34]

In principle, the nonirradiative decay of plasmons transfers part of the energy to the conduction electrons in gold, generating "hot electrons" that can escape from the metal surface and directly take part in the reduction reaction. Under dark conditions, the Au superstructures catalyze the reduction reaction by facilitating the transfer of electrons from the reductant (BH_4^- in this experiment) to $-NO_2$ via an intermediate state. Upon illumination of visible light, surface plasmons of Au superstructures are excited, providing an extra channel for the electron transfer. On the basis of the experimental data and SPR analysis, an operating mechanism is identified for visible-light-accelerated catalytic reactions over

DOI: 10.1021/acsami.5b01078
ACS Appl. Mater. Interfaces 2015, 7, 8200−8208

Au superstructures (Figure 5). As discussed above, the Au superstructures show strong broadband visible light absorption due to their plasmon resonance coupling (Figure 5I). This process enables a high concentration of photon flux energy in a small volume of the plasmonic Au nanostructures. The enhanced light energy utilization can further excite plasmons and generate even more hot electrons from gold conduction band. As a consequence, more separated electron−hole pairs are formed in turn at gold interfaces, creating more effective charge separation and active catalytic centers (Figure 5 II). In fact, as reported, effective charge separation can be realized even at a single metal nanoparticle under light energy excitation.[27] In this fashion, the free hot electrons of Au transfer directly to LUMO of the p-NP molecules. Meanwhile, the holes left in the separated energy band are injected by electrons from HOMO of BH_4^- ions (Figure 5II bottom). Thus, electron transfer from BH_4^- ions to p-NP molecules is realized through Au superstructures driven by visible light. In this process, the enhanced effective charge separation on the superstructure surfaces not only decreases the activation energy (E_a) of the catalytic reaction, but also boosts the reaction rate simultaneously. It is noted that the electrons and holes induced through the surface plasmon excitation are generated on the metal surfaces, which can avoid the long-range transport of charges and recombination of electron−hole pairs in the bulk phase. This characteristic behavior gives great advantage for catalytic reactions that occur at the interfaces of reactants and catalysts. Another possibility of thermal effect due to light energy can be understood by considering the local temperature elevation around Au superstructure surfaces via visible-light irradiation, although the catalytic reactions are conducted at constant temperature using a water bath. This may give rise to an increased reaction rate by the thermally activated process. As is known, temperature alteration of the reaction system cannot change the reaction pathway as well as the reaction energy. Therefore, E_a is a temperature-independent parameter[34] and should remain unchanged during reaction in this case. It appears inconsistent with our calculations that the E_a value is reduced with visible light irradiation. In addition, the experimental results from p-NP reduction conducted without using Au catalysts under dark or visible light irradiation, show only a negligible difference in reaction rate (Figure S3 in the Supporting Information). These results suggest a photonically induced mechanism, other than the photothermal effect, that plays a dominant role in the visible-light-enhanced catalytic performance.

CONCLUSION

In conclusion, a series of novel light-concentrating Au superstructures have been developed via a well-designed strategy and demonstrated significantly visible light-enhanced catalytic performance. The Au superstructures with dense assembly of Au nanostructures on surface of SiO_2 nanospheres are found to be responsible for enhanced broadband visible-light utilization because of plasmon resonance coupling. The plasmonic Au superstructures with increased photon energy utilization and effective electron−hole separation result in enhanced catalytic efficiency for p-NP reduction. An important relationship is established between the unconventional photoelectric properties of noble metals and their plasmonic nanostructures. These novel superstructures will pave a new way to developing metallic catalytic devices and related energy applications.

ASSOCIATED CONTENT

Supporting Information

XRD pattern (Figure S1), EDS spectrum (Figure S2), TEM images (Figure S3), recycling catalytic tests under visible light (Figure S5) and SEM image (Figure S6) of Au superstructures, Au amount determination by ICP-MS (Table S1), catalytic performance comparison under dark and visible light in the absence of catalyst (Figure S4), and related catalytic data for Ea calculations (Figures S7−S9 and Table S2). This material is available free of charge via the Internet at http://pubs.acs.org.

AUTHOR INFORMATION

Corresponding Authors

*Fax: 86-021-65983706. Tel: 86-021-65988029. E-mail: yangjinhu2010@gmail.com.
*E-mail: lilyqin@tongji.edu.cn
*E-mail: donglu.shi@uc.edu.

Notes

The authors declare no competing financial interest.

ACKNOWLEDGMENTS

This work was financially supported by National Natural Science Foundation (21273161 and 21101117), The Program for Professor of Special Appointment (Eastern Scholar) at Shanghai Institutions of Higher Learning, Shanghai Innovation Program (13ZZ026), Scientific Research Foundation for the Returned Overseas Chinese Scholars of SEM, and the Fundamental Research Funds for the Central Universities.

REFERENCES

(1) Mahmoud, M. A.; Saira, F.; El-Sayed, M. A. Experimental Evidence for the Nanocage Effect in Catalysis with Hollow Nanoparticles. *Nano Lett.* **2010**, *10*, 3764−3769.
(2) Lee, J.; Park, J. C.; Song, H. A Nanoreactor Framework of a Au@SiO_2 Yolk/shell Structure for Catalytic Reduction of P-Nitrophenol. *Adv. Mater.* **2008**, *20*, 1523−1528.
(3) Guo, X.; Zhang, Q.; Sun, Y. H.; Zhao, Q.; Yang, J. Lateral Etching of Core-shell Au@metal Nanorods to Metal-tipped Au Nanorods with Improved Catalytic Activity. *ACS Nano* **2012**, *6*, 1165−1175.
(4) Ding, M. G.; Sorescu, D. C.; Kotchey, G. P.; Star, A. Welding of Gold Nanoparticles on Graphitic Templates for Chemical Sensing. *J. Am. Chem. Soc.* **2012**, *134*, 3472−3479.
(5) Joseph, V.; Engelbrekt, C.; Zhang, J. D.; Gernert, U.; Ulstrup, J.; Kneipp, J. Characterizing the Kinetics of Nanoparticle-catalyzed Reactions by Surface-enhanced Raman Scattering. *Angew. Chem., Int. Ed.* **2012**, *51*, 7592−7596.
(6) Du, J.; Qi, J.; Wang, D.; Tang, Z. Y. Facile Synthesis of Au@TiO_2 Core−shell Hollow Spheres for Dye-sensitized Solar Cells with Remarkably Improved Efficiency. *Energy Environ. Sci.* **2012**, *5*, 6914−6918.
(7) Cláudia, G. S.; Juárez, R.; Marino, T.; Molinari, R.; García, H. Influence of Excitation Wavelength (UV or Visible light) on the Photocatalytic Activity of Titania Containing Gold Nanoparticles for the Generation of Hydrogen or Oxygen from Water. *J. Am. Chem. Soc.* **2011**, *133*, 595−602.
(8) Armbrüster, M.; Kovnir, K.; Friedrich, M.; Teschner, D.; Wowsnick, G.; Hahne, M.; Gille, P.; Szentmiklósi, L.; Feuerbacher, M.; Heggen, M.; Girgsdies, F.; Rosenthal, D.; Schlogl, R.; Grin, Y. $Al_{13}Fe_4$ as a Low-cost Alternative for Palladium in Heterogeneous Hydrogenation. *Nat. Mater.* **2012**, *11*, 690−693.
(9) Li, B. J.; Xu, Z. A Nonmetal Catalyst for Molecular Hydrogen Activation with Comparable Catalytic Hydrogenation Capability to Noble Metal Catalyst. *J. Am. Chem. Soc.* **2009**, *131*, 16380−16382.

DOI: 10.1021/acsami.5b01078
ACS Appl. Mater. Interfaces 2015, 7, 8200−8208

(10) Guo, S. J.; Sun, S. H. FePt Nanoparticles Assembled on Graphene as Enhanced Catalyst for Oxygen Reduction Reaction. *J. Am. Chem. Soc.* **2012**, *134*, 2492−2495.
(11) Guo, S. J.; Zhang, S.; Sun, X. L.; Sun, S. H. Synthesis of Ultrathin FePtPd Nanowires and Their Use as Catalysts for Methanol Oxidation Reaction. *J. Am. Chem. Soc.* **2011**, *133*, 15354−15357.
(12) Esswein, A. J.; Nocera, D. G. Hydrogen Production by Molecular Photocatalysis. *Chem. Rev.* **2007**, *107*, 4022−4047.
(13) Zhao, L. B.; Huang, Y. F.; Liu, X. M.; Anema, J. R.; Wu, D. Y.; Ren, B.; Tian, Z. Q. A DFT Study on Photoinduced Surface Catalytic Coupling Reactions on Nanostructured Silver: Selective Formation of Azobenzene Derivatives from Para-substituted Nitrobenzene and Anilinew. *Phys. Chem. Chem. Phys.* **2012**, *14*, 12919−12929.
(14) Zhu, H. Y.; Ke, X. B.; Yang, X. Z.; Sarina, S.; Liu, H. W. Reduction of Nitroaromatic Compounds on Supported Gold Nanoparticles by Visible and Ultraviolet Light. *Angew. Chem., Int. Ed.* **2010**, *49*, 9657−9661.
(15) Xu, P.; Kang, L. L.; Mack, N. H.; Schanze, K. S.; Han, X. J.; Wang, H. L. Mechanistic Understanding of Surface Plasmon Assisted Catalysis on a Single Particle: Cyclic Redox of 4-aminothiophenol. *Sci. Rep.* **2013**, *3*, 2997 DOI: 10.1038/srep02997.
(16) Fountoulaki, S.; Daikopoulou, V.; Gkizis, P. L.; Tamiolakis, I.; Armatas, G. S.; Lykakis, I. N. Mechanistic Studies of the Reduction of Nitroarenes by $NaBH_4$ or Hydrosilanes Catalyzed by Supported Gold Nanoparticles. *ACS Catal.* **2014**, *4*, 3504−3511.
(17) Shin, H.-S.; Huh, S. Au/Au@Polythiophene Core/Shell Nanospheres for Heterogeneous Catalysis of Nitroarenes. *ACS Appl. Mater. Interfaces* **2012**, *4*, 6324−6331.
(18) Dotzauer, D. M.; Bhattacharjee, S.; Wen, Y.; Bruening, M. L. Nanoparticle-Containing Membranes for the Catalytic Reduction of Nitroaromatic Compounds. *Langmuir* **2009**, *25*, 1865−1871.
(19) Wu, S.; Dzubiella, J.; Kaiser, J.; Drechsler, M.; Guo, X. H.; Ballauff, M.; Lu, Y. Thermosensitive Au-PNIPA Yolk−Shell Nanoparticles with Tunable Selectivity for Catalysis. *Angew. Chem., Int. Ed.* **2012**, *51*, 2229−2233.
(20) Kuroda, K.; Ishida, T.; Haruta, M. Reduction of 4-nitrophenol to 4-aminophenol over Au Nanoparticles Deposited on PMMA. *J. Mol. Catal. A-Chem.* **2009**, *298*, 7−11.
(21) Fujishima, A.; Honda, K. Electrochemical Photolysis of Water at A Semiconductor Electrode. *Nature* **1972**, *238*, 37−38.
(22) Asahi, R.; Morikawa, T.; Ohwaki, T.; Aoki, K.; Taga, Y. Visible-light Photocatalysis in Nitrogen-doped Titanium Oxides. *Science* **2001**, *293*, 269−271.
(23) Barnes, W. L.; Dereux, A.; Ebbesen, T. W. Surface Plasmon Subwavelength Optics. *Nature* **2003**, *424*, 824−830.
(24) Tsai, C. Y.; Lin, J. W.; Wu, C. Y.; Lin, P. T.; Lu, T. W.; Lee, P. T. Plasmonic Coupling in Gold Nanoring Dimers: Observation of Coupled Bonding Mode. *Nano Lett.* **2012**, *12*, 1648−1654.
(25) Su, K.-H.; Wei, Q.-H.; Zhang, X.; Mock, J. J.; Smith, D. R.; Schultz, S. Interparticle Coupling Effects on Plasmon Resonances of Nanogold Particles. *Nano Lett.* **2003**, *3*, 1087−1090.
(26) Hutter, E.; Fendler, J. H. Exploitation of Localized Surface Plasmon Resonance. *Adv. Mater.* **2004**, *16*, 1685−1706.
(27) Ghosh, S. K.; Pal, T. Interparticle Coupling Effect on the Surface Plasmon Resonance of Gold Nanoparticles: from Theory to Applications. *Chem. Rev.* **2007**, *107*, 4797−4862.
(28) Ye, J.; Pol, V. D. Plasmonic Behaviors of Gold Dimers Perturbed by Single Nanoparticle in the Gap. *Nanoscale* **2012**, *4*, 7205−7211.
(29) Knight, M. W.; Sobhani, H.; Nordlander, P.; Halas, N. J. Photodetection with Active Optical Antennas. *Science* **2011**, *332*, 702−704.
(30) César, C. Plasmon-induced Hot-electron Generation at Nanoparticle/metal-oxide Interfaces for Photovoltaic and Photocatalytic Devices. *Nat. Photonics* **2014**, *8*, 95−103.
(31) Langille, M. R.; Personick, M. L.; Zhang, J.; Mirkin, C. A. Bottom-up Synthesis of Gold Octahedra with Tailorable Hollow Features. *J. Am. Chem. Soc.* **2011**, *133*, 10414−10417.
(32) Sun, F.; Yu, J. C. Photochemical Preparation of Two-dimensional Gold Spherical Pore and Hollow Sphere Arrays on a Solution Surface. *Angew. Chem., Int. Ed.* **2007**, *46*, 773−777.
(33) Jin, M. S.; Liu, H. Y.; Zhang, H.; Xie, Z. X.; Liu, J. Y.; Xia, Y. N. Synthesis of Pd Nanocrystals Enclosed by {100} Facets with Sizes <10 nm for Application in CO Oxidation. *Nano Res.* **2011**, *4*, 83−91.
(34) Zeng, J.; Zhang, Q.; Chen, J.; Xia, Y. N. A Comparison Study of The Catalytic Properties of Au-based Nanocages, Nanoboxes, and Nanoparticles. *Nano Lett.* **2010**, *10*, 30−35.
(35) Furube, A.; Du, L.; Hara, K.; Katoh, R.; Tachiya, M. Ultrafast Plasmon-induced Electron Transfer from Gold Nanodots into TiO_2 Nanoparticle. *J. Am. Chem. Soc.* **2007**, *129*, 14852−14853.
(36) Zuo, Y. H.; Qin, Y.; Jin, C.; Li, Y.; Shi, D. L.; Wu, Q. S.; Yang, J. H. Double-side ZnO Nanorod Arrays on Single-crystal Ag Holed Microdisks with Enhanced Photocataltytic Efficiency. *Nanoscale* **2013**, *5*, 4388−4394.
(37) Wang, P.; Huang, B. B.; Dai, Y.; Whangbo, M. H. Plasmonic Photocatalysts: Harvesting Visible Light with Noble Metal Nanoparticles. *Phys. Chem. Chem. Phys.* **2012**, *14*, 9813−9825.
(38) Zheng, Z. K.; Huang, B. B.; Qin, X. Y.; Zhang, X. Y.; Dai, Y.; Whangbo, M. H. Facile In Situ Synthesis of Visible-light Plasmonic Photocatalysts M@TiO_2 (M = Au, Pt, Ag) and Evaluation of Their Photocatalytic Oxidation of Benzene to Phenol. *J. Mater. Chem.* **2011**, *21*, 9079−9087.
(39) Wang, S. W.; Yu, Y.; Zuo, Y. H.; Li, C. Z.; Yang, J. H.; Lu, C. H. Synthesis and Photocatalysis of Hierarchical Heteroassemblies of ZnO Branched Nanorod Arrays on Ag Core Nanowires. *Nanoscale* **2012**, *4*, 5895−5901.
(40) Christopher, P.; Xin, H.; Linic, S. Visible-light-enhanced Catalytic Oxidation Reactions on Plasmonic Silver Nanostructures. *Nat. Chem.* **2011**, *3*, 467−472.
(41) Stöber, W.; Fink, A.; Bohn, E. Controlled Growth of Monodisperse Silica Spheres in the Micron Size Range. *J. Colloid Interface Sci.* **1968**, *26*, 62−69.
(42) Westcott, S. L.; Oldenburg, S. J.; Lee, T. R.; Halas, N. J. Formation and Adsorption of Clusters of Gold Nanoparticles onto Functionalized Silica Nanoparticle Surfaces. *Langmuir* **1998**, *14*, 5396−5401.
(43) Wang, H.; Halas, N. J. Mesoscopic Au "Meatball" Particles. *Adv. Mater.* **2008**, *20*, 820−825.
(44) Bao, H.; Butz, B.; Zhou, Z.; Spiecker, E.; Hartmann, M.; Taylor, R. N. K. Silver-Assisted Colloidal Synthesis of Stable, Plasmon Resonant Gold Patches on Silica Nanospheres. *Langmuir* **2012**, *28*, 8971−8978.
(45) Li, Y.; Zu, L. H.; Liu, G. L.; Qin, Y.; Shi, D. L.; Yang, J. H. Nanospherical Surface-Supported Seeded Growth of Au Nanowires: Investigation on a New Growth Mechanism and High-Performance Hydrogen Peroxide Sensors. *Part. Part. Syst. Charact.* **2014**, DOI: 10.1002/ppsc.201400200.
(46) Xie, W.; Walkenfort, B.; Schlücker, S. Label-free SERS Monitoring of Chemical Reactions Catalyzed by Small Gold Nanoparticles using 3D Plasmonic Superstructures. *J. Am. Chem. Soc.* **2013**, *135*, 1657−1660.
(47) Lee, A.; Andrade, G. F. S.; Ahmed, A.; Souza, M. L.; Coombs, N.; Tumarkin, E.; Liu, K.; Gordon, R.; Brolo, A. G.; Kumacheva, E. Probing Dynamic Generation of Hot-spots in Self-assembled Chains of Gold Nanorods by Surface-enhanced Raman Scattering. *J. Am. Chem. Soc.* **2011**, *133*, 7563−7570.
(48) Schmit, V. L.; Martoglio, R.; Scott, B.; Strickland, A. D.; Carron, K. T. Lab-on-a-bubble: Synthesis, Characterization, and Evaluation of Buoyant Gold Nanoparticle-coated Silica Spheres. *J. Am. Chem. Soc.* **2012**, *134*, 59−62.
(49) Sivapalan, S. T.; DeVetter, B. M.; Yang, T. K.; van Dijk, T.; Schulmerich, M. V.; Carney, P. S.; Bhargava, R.; Murphy, C. J. Off-resonance Surface-enhanced Raman Spectroscopy from Gold Nanorod Suspensions as a Function of Aspect Ratio: Not What We Thought. *ACS Nano* **2013**, *7*, 2099−2105.
(50) Lu, W. T.; Singh, A. K.; Khan, S. A.; Senapati, D.; Yu, H. T.; Ray, P. C. Gold Nano-popcorn-based Targeted Diagnosis, Nano-

DOI: 10.1021/acsami.5b01078
ACS Appl. Mater. Interfaces 2015, 7, 8200−8208

therapy Treatment, and In Situ Monitoring of Photothermal Therapy Response of Prostate Cancer Cells Using Surface-enhanced Raman Spectroscopy. *J. Am. Chem. Soc.* **2010**, *132*, 18103−18114.
(51) Kong, X. M.; Yu, Q.; Zhang, X. F.; Du, X. Z.; Gong, H.; Jiang, H. Synthesis and Application of Surface Enhanced Raman Scattering (SERS) Tags of Ag@SiO_2 Core/shell Nanoparticles in Protein Detection. *J. Mater. Chem.* **2012**, *22*, 7767−7774.
(52) Sahiner, N.; Kaynak, A.; Butun, S. Soft Hydrogels for Dual Use: Template for Metal Nanoparticle Synthesis and a Reactor in the Reduction of Nitrophenols. *J. Non-Cryst. Solids* **2012**, *358*, 758−764.
(53) Sahiner, N.; Butun, S.; Ozay, O.; Dibek, B. Utilization of Smart Hydrogel−Metal Composites as Catalysis Media. *J. Colloid Interface Sci.* **2012**, *373*, 122−128.
(54) Sahiner, N.; Yildiz, S.; Al-Lohedan, H. The Resourcefulness of p(4-VP) Cryogels as Template for In Situ Nanoparticle Preparation of Various Metals and Their Use in H_2 Production, Nitrocompound Reduction and Dye Degradation. *Appl. Catal., B* **2015**, *166−167*, 145−154.

DOI: 10.1021/acsami.5b01078
ACS Appl. Mater. Interfaces 2015, 7, 8200−8208